Low-Temperature Aqueous Batteries: Challenges and Opportunities

Yiming Sui, Mingliang Yu, Yunkai Xu, and Xiulei Ji*

Department of Chemistry, Oregon State University, Corvallis, OR, 97331-4003, United States * david.ji@oregonstate.edu

Abstract

Aqueous batteries represent promising candidates to address the grand challenge of energy storage. Ideally, a battery ought to deliver performance at low temperatures. Unfortunately, water has a high freezing point of 0 °C at 101 KPa, where the limited low-temperature performance of aqueous batteries is usually expected. However, significant progress has been made recently in suppressing the freezing point of aqueous electrolytes, which leads to the demonstration of some low-temperature aqueous batteries. This article summarizes the challenges in low-temperature aqueous batteries as well as the reported strategies in promoting the low-temperature performance of these batteries.

1. Introduction

Aqueous batteries are at the focal point to meet the demand for energy storage so that more renewable energy can be installed. Aqueous batteries have the advantages of low cost, minimal environmental impacts, and non-flammability, which render such batteries conducive for gridscale applications. Depending on the applications, the operation conditions of batteries may vary dramatically, where the temperature is a primary consideration. Competitive battery technologies need to deliver acceptable performance at extremely low temperatures at locations such as polar regions, high altitude locales, and outer space. For such applications, a basic requirement of aqueous batteries that employ liquid electrolytes is that the electrolyte should not be frozen. Electrolyte freezing may lead to many dire consequences such as salt precipitation, volume expansion of the electrolyte and the associated deformation of the batteries, and the failure of providing power at a requisite current rate. To date, the primary strategies to tackle the challenge include 1) adding salt additives, e.g., 20 m LiTFSI², 2) adding organic additives or co-solvents, e.g., dimethyl sulfoxide (DMSO)³, and 3) using hydrogels as the electrolyte, e.g., polyacrylic acid (PAA) hydrogel.⁴⁻⁸ Through these approaches, the chemical environment of water molecules is controlled to reduce the freezing point of aqueous electrolytes, where a major task is to mitigate the extent of H-bonding between adjacent water molecules. Thus, water molecules do not readily nucleate into an ordered tetrahedral structure, i.e., with the DDAA (D: proton donor, A: proton acceptor) configuration, as commonly observed in ice.

Complementary to the recently published reviews on the topic of low-temperature aqueous batteries⁹⁻¹¹, this perspective is expected to highlight the basics pertinent to the topic, including the mechanism of electrolyte freezing and anti-freezing strategies as well as the kinetics-related issues and remedy approaches (Figure 1). Lastly, we will provide a perspective on the future development of aqueous batteries at low temperatures.

2. Electrolyte Freezing

2.1 The Basics of Freezing of Aqueous Solutions

The phase transition behavior from liquid water to solid ice under different conditions is an intricate phenomenon.^{12, 13} The flexible H-bond between water molecules results in the facile rearrangement of the local structure, thus generating polymorphs of ice at different temperatures and pressures (Figure 2a).¹²⁻¹⁴ For example, under the ambient pressure (101 KPa), pure water undergoes the solidification process into the Phase I ice at around 273 K, which exhibits an orthorhombic structure with a space group of Cmc2₁.^{13, 15}

Water molecules connect through directional H-bonds no matter their physical states in liquid or solid. A fully H-bonded water molecule is surrounded by four water molecules, forming a tetrahedral structure, known as DDAA (Figure 2b).¹⁶ The crystalline ice is rich in DDAA, and different phases of ice are distinguishable based on their unique stacking sequences of DDAA units. In contrast to solid, water molecules in the liquid state also have other H-bonded configurations, including partially H-bonded ones, *i.e.*, DDA, DAA, and DA, and the non-H-bonded, *i.e.*, free water (Figure 2b, c).¹⁷

Fourier Transform Infrared spectroscopy (FTIR) and Raman spectroscopy are the most used techniques to characterize the chemical environment of water molecules in electrolytes. They can distinguish O-H vibration modes in H-bonded structures. Under ambient conditions (101 KPa, 293 K), a Raman spectrum of pure water is shown in Figure 2c, where the five fitted peaks at 3041, 3220, 3430, 3572, and 3636 cm⁻¹ correspond to the O-H stretching modes in DAA, DDAA, DA, DDA, and free water, respectively. 16 Furthermore, strong H-bonding confines the vibration of O-H bonds, corresponding to lower vibration frequencies, thus the O-H stretching modes are classified into three types, including 1) strongly H-bonded (DAA, DDAA), 2) medium H-bonded (DA), and 3) weakly H-bonded (DDA and free water molecules). In addition to liquid and ice states, water can be in its supercooled state, where it remains as liquid below the freezing temperature. As a liquid, the supercooled water presents numerous unique features. For example, the internal tetrahedral DDAA structure contributes to a lower density, and interestingly, the supercooled water dissolves hydrophobic molecules better. 16, 18, 19 On the other hand, the supercooled water has a larger surface tension, where from room temperature to -23 °C, the surface tension increases by 10%. 19 Note that the increased surface tension may negatively affect the electrolyte wettability on separators and electrodes, which may harm the kinetics of batteries.

There are plentiful factors that affect the freezing point of water such as the composition, *e.g.*, salt^{20, 21}, co-solvent³, and nanophase additive,^{22, 23} and the size of water domains²⁴. For example, dissolving salts in water can effectively interrupt the H-bonding structure because the dissociated ions interact with water molecules more strongly than that between water molecules. Similarly, introducing co-solvents is also effective in breaking the original H-bond structure. In both cases, the scale of the DDAA structure is reduced significantly, which, thus, suppresses the transition of the disordered H-bonded structure in liquid water to the ordered DDAA ice solid. From the phase diagram perspective, these additives reduce the partial vapor pressure of water; hence, the freezing point needs to decrease to reach the equilibrium between ice/water phases.²⁵ In addition, the nanosized water domains in the confined space can alter water's structural preference.²⁶ This is originated from the directional nature of the H-bond, which makes the H-bonding motifs non-distortable; thus, this phenomenon becomes significant only in a specific size range.

Overall, the phase diagrams and vibrational spectroscopies can help us understand water's freezing process and design practical anti-freezing strategies in aqueous batteries. To be specific, the freezing points of aqueous electrolytes can be manipulated by designing water's chemical environment by controlling the composition of electrolytes. The reported solutions to the freezing problem will be reviewed in the section below.

2.2 Anti-freezing Strategies

As mentioned above, the freezing process of water is closely correlated to its chemical environment, particularly the different configurations of H-bonds. Microscopically, it requires four coordinated water molecules to form the ordered DDAA structure in ice. Therefore, the reported anti-freezing methods in the battery field have primarily focused on changing the H-bonding structure in aqueous electrolytes, thus suppressing the formation of the DDAA structure. The specific strategies include adding salt additives or organic additives and using hydrogel electrolytes. Herein, we will only discuss selected works to highlight the related fundamental aspects.

2.2.1 Salt Additives

Adding soluble salts into water is a well-known strategy to decrease the freezing point of water by breaking the H-bonding conditions. For instance, metal chlorides are common de-icing reagents to melt the ice on roads in winter.²⁷ In the aqueous battery field, this method is also broadly applied to extend the liquid window of water to low temperatures, while the mutual interaction between dissociated cations, anions, and water solvents directly determines the effectiveness of lowering the freezing point of aqueous electrolytes (Figure 3a).

First, metal cations could interact strongly with water molecules through ion-dipole interactions.²⁸ The solvation of ions by water molecules causes the salt dissociation and hydration of ions. The solvated ions reside in a core-shell structure surrounded by the first and most likely

the second solvation shells, beyond which there exist the free water molecules (Figure 3b).²⁹ To avoid confusion, it should be noted that the free water here refers to those free of interaction with ions, as opposed to the water free of H-bonding mentioned earlier. To summarize, the ion type affects the interaction strength and the coordination number with aqua ligands. For example, Zn²⁺ with a higher charge density interacts more strongly with water than Li⁺ of a similar radius. Furthermore, the salt concentration also plays a critical role of determining the freezing point of aqueous electrolytes. An equation is commonly used to describe the freezing point depression as a function of the salt concentration:³⁰

$$\Delta T_f = T_{water} - T_{sol} = K_f \cdot m$$
 Equation 1

where T_{water} represents the freezing point of pure water, T_{sol} is the freezing point of the solution, K_f stands for the freezing point depression constant ($^{\sim}$ 1.86 $^{\circ}$ C kg mol⁻¹ for aqueous solution), and m is the dissociated ion concentration in molality. The equation works for simple salts, where, for example, adding 1 m LiCl into water could reduce the freezing point to -3.72 $^{\circ}$ C. However, the equation loses its accuracy to predict the freezing point of the solution when ions of salts form stronger H-bonds with water molecules $(e.g., SO_4^{2-})^{31}$ or change the dissociated states at different concentrations $(e.g., ZnCl_2)^{32,31}$, which will be discussed later.

The concentrated electrolyte is usually referred to as water-in-salt electrolytes (WiSE), when the concentration of salts reaches the level where the number of water molecules is only sufficient to form the primary hydration shell of the cations or the cations' hydration shell is incomplete. WiSE can widen the electrochemical stability window of aqueous electrolytes; however, WiSE is usually not compatible with low temperatures. In contrast, the deep eutectic solutions, as indicated in their phase diagrams, albeit relatively concentrated, can reach the lowest freezing points. For example, as shown in the phase diagram of the ZnCl₂/water binary system (Figure 3c), the lowest freezing temperature of -173 °C is realized at the eutectic composition of 7.5 m ZnCl₂. Further analysis suggested that the major species of the 7.5 m ZnCl₂ electrolyte include Zn(H₂O)₂Cl₄²⁻, ZnCl⁺, Zn(H₂O)₆²⁺, and some water molecules that interact between themselves through heavily interrupted H-bonds (Figure 3d).32 Upon approaching 7.5 m, the gradually interrupted H-bond structure helps suppress the formation of the ordered DDAA structure of water, thus reducing the freezing point. When further increasing the ZnCl₂ concentration, the trend reverses and the freezing point increases, which results from the stronger cation-anion interactions and the more facile salt precipitation. In fact, when the salt concentration exceeds 20 m, the electrolyte species are transformed to a mixture of $Zn(H_2O)_6^{2+}$, and $ZnCl_4^{2-}$, and $Zn-Cl_4^{2-}$ aggregates. According to the phase diagram, ice is not the solidification product of the electrolyte when C_{ZnCl_2} exceeds 7.5 m. Therefore, the eutectic composition of 7.5 m strikes a balance between the interrupted H-bonding network of water and the relatively weak cation-anion interaction strength, thus arriving at the extremely low freezing point.³² Similar situations like ZnCl₂ are also observed in other electrolytes such as Mg(ClO₄)₂³³, LiNO₃³⁴, MgCl₂²¹, and CaCl₂²¹ electrolytes, where the lowest freezing point appears at the eutectic compositions in the saltwater systems. Benefitting from the ultra-low freezing point, the 7.5 m ZnCl₂ electrolyte retains

an acceptable ionic conductivity of 1.79 mS cm⁻¹ at -60 °C and 0.02 mS cm⁻¹ at -100 °C.³² Furthermore, the Zn||Cu half-cell presents a high Coulombic efficiency of 99.53% at -70 °C, and the PANI||Zn full cell delivers a reversible capacity of ~100 mAh g⁻¹ at a current rate of 20 mA g⁻¹ at -70 °C.³²

In addition to $ZnCl_2$, other highly soluble salts have also been reported in different types of aqueous batteries for low-temperature applications. For instance, Ramanujapuram and Yushin reported that saturated LiCl (~16 m)-based cells could stably operate at -40 °C with over 72% capacity retention relative to that at room temperature;³⁰ a LiTFSI electrolyte (21 m) enables the Li₃V₂(PO₄)₃ | LiTi₂(PO₄)₃ full cell, which delivers a high capacity of 111 mAh g⁻¹ reversibly at -20 °C;² Lu and Hu *et al.* reported that a 22 m KCF₃SO₃ electrolyte³⁵ facilitates an aqueous K-ion battery to operate at -20 °C, and the Coulombic efficiency is considerably higher at low temperatures than that at high temperatures (*e.g.*, 60 °C).

Unlike the cations, anion changes the H-bonding structure of water molecules through two different routes. Firstly, it is reported that the oxygen and fluoride-containing anions (e.g., SO_4^{2-} , PO_4^{3-} , BF_4^{-})^{31,36,37} could directly form H-bonds with water molecules in acidic conditions, and the bonding strength increases at lower pH values.³⁸ Impressively, dilute H_2SO_4 electrolytes with a concentration < 3 M in the study of Niu et~al. exhibits an extremely low freezing point of -70 °C.³¹ Raman spectra confirm the destruction of the original H-bonding structure between water molecules, as suggested by the diminished peaks of the O-H stretching modes between 3000 and 3600 cm⁻¹ (Figure 4a). Meanwhile, the emerging and gradually strengthened peak at around 960 cm⁻¹ at higher H_2SO_4 concentrations indicates the stronger H-bonding connection between SO_4^{2-} and water molecules (Figure 4a). It was demonstrated that the proton cells with 5 M H_2SO_4 electrolyte could deliver reversible performance at -70 °C.

In addition, whether anions form ion pairs with cations can alter the extent of H-bonding between water molecules, which affects whether water molecules are allowed to fully hydrate cations. According to Liang and Chou *et al.*, the primary factor is the anion's most negative electrostatic potential (ESP), where ESP is defined as the work done to move a unit positive charge from infinity to the considered point of anions.³⁹ Its value indicates the binding energy between cations or H_2O and anions, where according to the DFT calculations, the cation and anion interaction is stronger than that of the anion- H_2O interaction. Therefore, anions with more negative ESPs are more likely to coordinate cations in the first coordination shell, which reduces the water coordination number around cations; thus, the melting point is higher. Conversely, introducing anions with a less negative ESP value may increase the number of the fully hydrated cations in the electrolytes, *e.g.*, $Zn(H_2O)_6^{2+}$, thus interrupting the H-bonding structure between water molecules, thus lowering the melting point. In the same study, the DFT calculations reveal the ESP trend of several anions with the common cation of Zn^{2+} : $SO_4^{2-} < NO_3^- < Cl^- < l^- < CF_3SO_3^-$, which is consistent with the trend of decreasing freezing point in solutions, respectively (Figure 4b, c).³⁹ Further MD calculations and Raman results corroborate that there are the highest

 $Zn(H_2O)_6^{2+}$ amount and the lowest amount of strong H-bonded water in $Zn(CF_3SO_3)_2$ electrolytes (Figure 4d). The cell based on the 2 M $Zn(CF_3SO_3)_2$ electrolyte could reversibly function at -30 °C.

2.2.2 Co-solvent

Introducing organics into aqueous electrolytes as co-solvents or additives is another strategy to suppress water freezing. Similar to polyanions, the reduced freezing point also originates from the new H-bonds between the organics and water molecules, which weakens/reduces the Hbonds between water molecules. Common anti-freezing organic additives contain DMSO³ and ethylene glycol (EG)⁴⁰⁻⁴². These co-solvents usually possess high polarity; hence they are miscible with water in various ratios. In fact, the trend of freezing point reduction is not negatively proportional to the mass ratio of the co-solvent in the mixture but more possibly presents a Vshape relationship. This is similar to the eutectic compositions of binary water-salt mixtures. For example, pure EG possesses a high freezing point of -13 °C, and the freezing point reaches the minimum of -33 °C at the composition of EG: H₂O 60:100 in V: V.⁴⁰ Furthermore, the electrolyte of 2 M ZnSO₄ solvated by the EG/water mixture with a volume ratio of 40% possesses a high ionic conductivity of 6.9 mS cm⁻¹ at -40 °C. More impressively, when water and DMSO are mixed at a molar fraction (χ) of 0.3, the freezing point is dramatically reduced to -130 °C, much lower than that of pure DMSO (18.9 °C). 43 In addition, 2 M NaClO₄ further reduces the freezing point to below -150 °C.⁴³ In comparison, higher or lower molar fractions of DMSO raise the freezing point. MD simulation demonstrates that 1DMSO-2H₂O is the basic bonding unit in the γ_{DMSO} =0.3 electrolyte, which may allow the most extent of water molecule trapping.³ Besides, the 1DMSO-2H₂O complex is possibly a eutectic phase (DMSO hydrate) that can crystallize at an extremely low temperature, similar to the ZnCl₂-water system. Despite a relatively low ionic conductivity (~0.11 mS cm⁻¹) at -50 °C, the 2 M NaClO₄ χ_{DMSO}=0.3 electrolyte still allows AC | NaTi₂(PO₄)₃@C full cell to retain over 60% its capacity measured at 25 °C.

2.2.3 Hydrogels

Hydrogels usually serve as semi-solid-state electrolytes, where a solid polymeric skeleton retains a large amount of water inside through hydrophilic groups on surfaces. 44 More specifically, the polymer holds water molecules through H-bonds, which also plays the role of altering the H-bonded structure of water and decreasing the freezing point of bulk electrolytes. Therefore, the type of terminal groups of the polymer skeleton is one determining factor of the anti-freezing capability. For instance, DFT calculations demonstrate that the bonding strength between water molecules, between the hydroxyl group and water molecules in polyvinyl alcohol (PVA) hydrogel, and between the carboxyl group and water molecules in polyacrylic acid (PAA) hydrogel are -5.75, -6.11, and -12.92 kcal mol⁻¹, respectively. Furthermore, alkalified PAA with higher polarity contributes to higher binding energy with water molecules (-16.96 kcal mol⁻¹), thus significantly reducing the freezing point to -25 °C when comprising 10 wt.% KOH. In comparison, the PVA hydrogel containing 10 wt.% KOH freezes at a higher temperature -13 °C. The zinc-air cell based

on the electrolyte delivers a high specific capacity of 691 mAh $\rm g^{-1}$ at -20 °C, retaining over 92.7% of capacity under ambient conditions.⁴

Despite the improvement, the hydrogel strategy alone is not practical to solve the freezing problem.¹¹ This relates to the large pore size inside hydrogels. The accommodated water molecules could be generally divided into three types: 1) strongly bonded ones, which are located most closely to the polar groups and are the most difficult to freeze, 2) weakly bonded ones, which are farther to the first type and get minor improvement in anti-freezing, and 3) free ones, which exhibit a similar structure as that in regular water electrolytes.⁴⁴ As the pore size gets larger, the type III water molecules play the dominant roles, and the impact of polar groups on the polymer skeleton will be largely weakened. Therefore, in most cases, the hydrogel strategy is combined with other anti-freezing strategies for applications at low temperatures such as WiSE^{4,} and organic co-solvents^{46, 47}.

3. Ionic Conductivity

According to the Arrhenius equation, ionic conductivity is a thermally activated process; lower temperatures would significantly decrease ionic conductivity and increase reaction polarization. Electrochemical impedance spectroscopy (EIS) results can reveal the higher charge-transfer resistance at low temperatures. The problems become more severe in some highly concentrated electrolytes, where the strong electrostatic force between crowded cations and between cations and water molecules retards the diffusion of the cation charge carriers. Accordingly, several strategies are applicable to increase the ionic conductivity and maintain the anti-freezing properties, including localized WiSE and alternative charge carriers.

3.1 Localized Water-in-Salt Electrolytes

The localized solvent-in-salt electrolytes have been broadly studied in organic-electrolyte-based lithium-metal batteries, but the concept is still at its infancy in the field of low-temperature aqueous batteries. Decalized WiSE can be prepared by introducing an electrochemically inert solvent into WiSE. The co-solvent should exhibit a low donor number (DN) and could be aprotic, which means that they have weak binding with water molecules and could not solvate cations (Figure 5a). As a complementary strategy to WiSE, the co-solvent addition will not change the original water-in-salt solvation structure, thus inheriting the advantages of WiSE, including the widened electrochemical stability window (Figure 5a, b). More importantly, the co-solvent would serve as a diluent to salt-water solvation complexes, thus reducing the electrostatic forces between ion complexes and improving the ionic conductivity. Macroscopically, the salt concentration decreases due to the increment of overall solvent volume, which significantly reduces the salt usage and costs for some expensive -imide salts (e.g., LiTFSI). For example, introducing a nonpolar diluent 1, 4-dioxane (1, 4-DX) into a WiSE (1 m Zn(TFSI)₂—19 m LiTFSI—9 m LiBETI in H₂O) could effectively reduce the viscosity from 577 mPa s to 24 mPa s and improve ionic conductivity from 2.1 mS cm⁻¹ to 3.3 mS cm⁻¹.51 Similar to ZnCl₂-based WiSE, the extremely

concentrated electrolyte presents a high freezing point of -2 °C, but the derived localized concentrated electrolyte shows a lower freezing point of -13 °C, which may relate to the new H-bonds between 1, 4-DX and water molecules. Furthermore, the S-N-S vibration of the imide salts in FTIR spectra undergoes a constant redshift with increasing the diluent concentration (Figure 5c). The FTIR results suggest that a higher concentration of the diluent increases the effective salt concentration in water, where anions replace water molecules in the inner solvation shells of Li⁺ ions. The stronger electrostatic interaction between Li⁺ and anions will weaken the S-N-S bonds inside the anions, which corresponds to the redshifts of S-N-S bonds in FTIR spectra. In addition, the destabilized bonds inside anions will promote their decomposition into SEI on the anode side. The localized WiSE also presents a lower contact angle over the Zn metal anode, namely better wettability than the pristine WiSE, which benefits the ion charge transfer across the electrode-electrolyte interface.

3.2 Alternative Charge Transfer Mechanisms

In aqueous electrolytes, the strong ion-dipole interactions between cations and water molecules and the electrostatic force between cations and anions facilitate the formation of the solvation structure, in which cations diffuse as the bulky complex ions, leading to the sluggish ionic diffusivity. As an alternative to metal cations, a proton is not only smaller and lighter but can conduct via the unique Grotthuss mechanism in aqueous electrolytes. Figure 6a schematically shows the Grotthuss mechanism—a structural diffusion, where when one H⁺ approaches one side of a water chain and forms a H-bond, and the spatial structure of H-bonded water molecules is shifted by conducting this H-bond. The H-bond is transferred to the other side of the water chain, thus kicking out another H⁺. The non-diffusion proton charge transfer process contributes to the superior ionic conductivity in acid solutions. More impressively, acids typically exhibit high solubility in the water solvent, and unlike inorganic metal salts, they will not precipitate even under sub-zero temperatures. In aqueous proton batteries, common acids are H₂SO₄^{31, 52} and H₃PO₄⁵³, partially due to their excellent stability and anti-freezing ability. For the H₂SO₄ solution, the optimal concentration of 5 M achieves a high ionic conductivity of 180 mS cm⁻¹ at 0 °C and still retains 120 mS cm⁻¹ and 30 mS cm⁻¹ at -40 °C and -70 °C, respectively (Figure 6b).³¹ And the eutectic composition of 9.5 m H₃PO₄ exhibits properties of the extremely low freezing point of -83 °C.53 Benefitted from the rapid ion diffusion kinetics, the full cell based on a Turnbull's blue analog Cu^{II}[Fe^{III}(CN)₆]_{2/3}·4H₂O cathode and MoO₃ anode retains its 55% capacity of room temperature at an extremely low temperature of -78 °C and suffers almost no capacity fading over 450 cycles at the rate of 25 mA g⁻¹.⁵³

4. Summary and Perspective

The renaissance of aqueous batteries is unfolding due to the intriguing properties of the aqueous electrolytes. The concerns over water freezing at low temperatures could be practically solved by changing the chemical environments around water molecules such as adding salts and organic co-solvents and applying hydrogel electrolytes. The strategies are to introduce another

component to the electrolyte to reduce the H-bonding interactions between water molecules, thus suppressing the transformation into the ordered DDAA structure of ice. However, the trend of the ratio of new components may not always be linear. The additives themselves may not possess low freezing points, but they could form eutectic phases with water such as $ZnCl_2$ and DMSO, which could achieve extremely low freezing points with mild concentrations. At the eutectic compositions, the additive-water mixture crystallizes as a single phase instead of experiencing the phase separation into frozen water (*i.e.*, ice) and additives. Besides, it should be noted that in the DMSO- H_2O eutectic mixture, even a low concentration of salt (2 M NaClO₄) could further decrease the freezing point from -130 °C to -150 °C. The fundamental explanation for the phenomenon is still lacking.

Besides the reported strategies, physical confinement is potentially another method to regulate the freezing behavior of water molecules at low temperatures. As mentioned above, hydrogen bonding is highly directional and non-flexible, which affects the size of different H-bonding structures. When the water molecules are confined in nano-channels, it is difficult for water molecules to transform into a DDAA structure and freeze into solid ice. For example, when confined in D \approx 1.2 nm hydrophilic nanopores, water's freezing point could be reduced to as low as -100 °C.²⁴ Raman spectra demonstrate the distinctly different patterns of O-H stretching bands of confined water from that of the bulk water (Figure 7a). Figure 7b shows the derived structure transformation process. The confined water displays a disordered structure at room temperature and undergoes more ordered alignment at low temperatures, yet remains liquid. Furthermore, further studies are warranted to reveal the impacts of other factors such as the pore size, pore structure, and physical/chemical properties of channel surfaces (*e.g.*, hydrophilicity) on the water's freezing behavior in confined space.^{26, 54, 55}

Kinetics is another critical factor for the performance of aqueous batteries at sub-zero temperatures. The challenge pertains to the reduced ionic conductivity within electrolytes at lower temperatures. Besides, fully hydrated ions that transport via the vehicular mechanism suffer from slow diffusion in electrolytes and large de-solvation energy before their insertion into electrodes. Caution should be taken that some anti-freezing strategies may aggravate the above problems. For instance, electrolytes of higher concentrations typically suffer from poor ionic conductivity, which could affect their electrochemical properties at low temperatures. Some strategies can potentially address this dilemma, including the localized WiSE⁵¹ and proton batteries³⁶. For proton batteries that employ the Grotthuss conduction, the diffusion-free charge transport renders such batteries a premium choice for low-temperature energy storage. Unfortunately, the reported aqueous proton batteries do not exhibit high energy density, where further progress is warranted. Meanwhile, other room-temperature strategies on improving ionic conductivity such as binary salt⁵⁶ remain unexplored in this field, which can be a good reference for improving kinetics for low-temperature aqueous batteries. In addition, lower temperatures increase the hydrogen bonding and surface tension of water, which results in higher contact angles of electrolytes on electrodes.^{8, 19, 57} The lowered wettability impedes the

diffusion rate and homogeneity of charge carriers on electrodes, resulting in high redox polarization and even provoking dendrite growth on metal anodes.^{58, 59} Unfortunately, the issue has received limited attention so far.⁵¹ Possible strategies including electrolyte additives⁵⁸ and electrode surface modifications^{60, 61} could be referred from room-temperature aqueous batteries and low-temperature batteries based on organic electrolytes. Similarly, other kinetic-limiting issues such as de-solvation energy and interphase formation (*i.e.*, SEI) are yet to be considered in the design of low-temperature aqueous electrolytes, which also needs more exploration in the future.

In addition, the practicality of designed strategies should be evaluated multi-dimensionally, including anti-freezing capability, ionic conductivity, cost, compatibility with electrodes, and *etc*. Furthermore, the solutions become meaningless when sacrificing the advantages of aqueous batteries. For example, high-cost electrolytes may not lead to commercialization. In contrast, economical salts, such as LiCl and ZnCl₂ are more promising options for low-cost aqueous batteries. In addition, introducing organic co-solvents are proven feasible solutions to expand electrochemical stability range and suppress electrolyte freezing for aqueous electrolytes, yet the hybrid electrolytes should not be flammable, thus not compromising the safety advantage.

Overall, the field of low-temperature aqueous batteries is still in its infancy. There is a great need for a fundamental understanding of the anti-freezing mechanisms and behavior of species in the electrolytes at low temperatures. It is expected that the integrated research with the rational design of electrolytes, advanced characterization, and simulation will help unveil the mechanisms and lead to the progress of batteries that will meet the demand for commercialization.

Acknowledgements:

X. Ji thanks U.S. National Science Foundation for the financial support with Awards CBET 2038381 and DMR 2004636.

References

- 1. Y. Sui and X. Ji, *Chemical Reviews*, **121**, 6654 (2021).
- 2. H. Wang, H. Zhang, Y. Cheng, K. Feng, X. Li and H. Zhang, Electrochimica Acta, 278, 279 (2018).
- 3. Q. Nian, J. Wang, S. Liu, T. Sun, S. Zheng, Y. Zhang, Z. Tao and J. Chen, *Angewandte Chemie International Edition*, **58**, 16994 (2019).
- 4. Z. Pei, Z. Yuan, C. Wang, S. Zhao, J. Fei, L. Wei, J. Chen, C. Wang, R. Qi and Z. Liu, *Angewandte Chemie*, **132**, 4823 (2020).
- 5. F. Mo, G. Liang, Q. Meng, Z. Liu, H. Li, J. Fan and C. Zhi, *Energy & Environmental Science*, **12**, 706 (2019).
- 6. Y. Huang, Z. Li, Z. Pei, Z. Liu, H. Li, M. Zhu, J. Fan, Q. Dai, M. Zhang and L. Dai, *Advanced Energy Materials*, **8**, 1802288 (2018).
- 7. J. Wei, G. Wei, Y. Shang, J. Zhou, C. Wu and Q. Wang, *Advanced Materials*, **31**, 1900248 (2019).
- 8. G. Gittens, Journal of Colloid and Interface Science, **30**, 406 (1969).
- 9. Q. Nian, T. Sun, S. Liu, H. Du, X. Ren and Z. Tao, *Chemical Engineering Journal*, **423**, 130253 (2021).

- 10. H. Wang, Z. Chen, Z. Ji, P. Wang, J. Wang, W. Ling and Y. Huang, *Materials Today Energy*, **19**, 100577 (2021).
- 11. Y. Zhao, Z. Chen, F. Mo, D. Wang, Y. Guo, Z. Liu, X. Li, Q. Li, G. Liang and C. Zhi, *Advanced Science*, **8**, 2002590 (2021).
- 12. E. Sanz, C. Vega, J. L. F. Abascal and L. G. MacDowell, *Physical Review Letters*, **92**, 255701 (2004).
- 13. S. Pipolo, M. Salanne, G. Ferlat, S. Klotz, A. M. Saitta and F. Pietrucci, *Physical review letters*, **119**, 245701 (2017).
- 14. Z. Zhang and X.-Y. Liu, *Chemical Society Reviews*, **47**, 7116 (2018).
- 15. A. Leadbetter, R. Ward, J. Clark, P. Tucker, T. Matsuo and H. Suga, *The Journal of chemical physics*, **82**, 424 (1985).
- 16. Q. Sun, Chemical Physics Letters, **568-569**, 90 (2013).
- 17. I. Đuričković, R. Claverie, P. Bourson, M. Marchetti, J.-M. Chassot and M. D. Fontana, *Journal of Raman Spectroscopy*, **42**, 1408 (2011).
- 18. Q. Sun, Chemical Physics Letters, **672**, 21 (2017).
- 19. V. Holten, C. Bertrand, M. Anisimov and J. Sengers, *The Journal of chemical physics*, **136**, 094507 (2012).
- 20. R. Bodnar, Geochimica et Cosmochimica acta, **57**, 683 (1993).
- 21. Y. Farnam, A. Wiese, D. Bentz, J. Davis and J. Weiss, *Construction and Building Materials*, **93**, 384 (2015).
- 22. H. Geng, X. Liu, G. Shi, G. Bai, J. Ma, J. Chen, Z. Wu, Y. Song, H. Fang and J. Wang, *Angewandte Chemie*, **129**, 1017 (2017).
- 23. H. Hong and W. Roy, in *Nanoengineering: Fabrication, Properties, Optics, and Devices IV*, p. 66451A (2007).
- 24. F. Alabarse, J. Haines, O. Cambon, C. Levelut, D. Bourgogne, A. Haidoux, D. Granier and B. Coasne, *Physical review letters*, **109**, 035701 (2012).
- 25. W. Xu, C. Liu, S. Ren, D. Lee, J. Gwon, J. C. Flake, T. Lei, N. Baisakh and Q. Wu, *Journal of Materials Chemistry A*, **9**, 25651 (2021).
- 26. K. Koga and H. Tanaka, The Journal of Chemical Physics, 122, 104711 (2005).
- 27. V. Padilla, P. Ghods and A. Alfantazi, *Construction and building materials*, **40**, 908 (2013).
- 28. B. Hribar, N. T. Southall, V. Vlachy and K. A. Dill, *Journal of the American Chemical Society*, **124**, 12302 (2002).
- 29. L. Suo, O. Borodin, T. Gao, M. Olguin, J. Ho, X. Fan, C. Luo, C. Wang and K. Xu, *Science*, **350**, 938 (2015).
- 30. A. Ramanujapuram and G. Yushin, Advanced Energy Materials, 8, 1802624 (2018).
- 31. F. Yue, Z. Tie, S. Deng, S. Wang, M. Yang and Z. Niu, *Angewandte Chemie*, **133**, 14001 (2021).
- 32. Q. Zhang, Y. Ma, Y. Lu, L. Li, F. Wan, K. Zhang and J. Chen, *Nature communications*, **11**, 1 (2020).
- 33. X. Bu, Y. Zhang, Y. Sun, L. Su, J. Meng, X. Lu and X. Yan, Journal of Energy Chemistry, 49, 198 (2020).
- 34. G. Ah-lung, B. Flamme, F. Ghamouss, M. Maréchal and J. Jacquemin, *Chemical Communications*, **56**, 9830 (2020).
- 35. L. Jiang, Y. Lu, C. Zhao, L. Liu, J. Zhang, Q. Zhang, X. Shen, J. Zhao, X. Yu and H. Li, *Nature Energy*, **4**, 495 (2019).
- 36. H. Jiang, W. Shin, L. Ma, J. J. Hong, Z. Wei, Y. Liu, S. Zhang, X. Wu, Y. Xu and Q. Guo, *Advanced Energy Materials*, **10**, 2000968 (2020).
- 37. T. Sun, H. Du, S. Zheng, J. Shi and Z. Tao, Advanced Functional Materials, 31, 2010127 (2021).
- 38. K. Tomikawa and H. Kanno, *The Journal of Physical Chemistry A*, **102**, 6082 (1998).
- 39. Q. Zhang, K. Xia, Y. Ma, Y. Lu, L. Li, J. Liang, S. Chou and J. Chen, ACS Energy Letters, 6, 2704 (2021).
- 40. N. Chang, T. Li, R. Li, S. Wang, Y. Yin, H. Zhang and X. Li, *Energy & Environmental Science*, **13**, 3527 (2020).

- 41. A. Tron, S. Jeong, Y. D. Park and J. Mun, ACS Sustainable Chemistry & Engineering, 7, 14531 (2019).
- 42. A. J. Roberts, A. F. Danil de Namor and R. C. T. Slade, *Physical Chemistry Chemical Physics*, **15**, 3518 (2013).
- 43. D. Rasmussen and A. MacKenzie, *Nature*, **220**, 1315 (1968).
- 44. B. Cursaru, P. O. Stanescu and M. Teodorescu, UPB Sci Bull Ser B, 72, 99 (2010).
- 45. H. Wang, J. Liu, J. Wang, M. Hu, Y. Feng, P. Wang, Y. Wang, N. Nie, J. Zhang, H. Chen, Q. Yuan, J. Wu and Y. Huang, *ACS Applied Materials & Interfaces*, **11**, 49 (2019).
- 46. F. Chen, D. Zhou, J. Wang, T. Li, X. Zhou, T. Gan, S. Handschuh-Wang and X. Zhou, *Angewandte Chemie*, **130**, 6678 (2018).
- 47. H. Gao, Z. Zhao, Y. Cai, J. Zhou, W. Hua, L. Chen, L. Wang, J. Zhang, D. Han and M. Liu, *Nature communications*, **8**, 1 (2017).
- 48. M. Petrowsky and R. Frech, *The Journal of Physical Chemistry B*, **113**, 5996 (2009).
- 49. S. Zhang, K. Xu and T. Jow, *Journal of Power Sources*, **115**, 137 (2003).
- 50. P. Zou, Y. Sui, H. Zhan, C. Wang, H. L. Xin, H.-M. Cheng, F. Kang and C. Yang, *Chemical Reviews*, **121**, 5986 (2021).
- 51. S. Chen, Q. Nian, L. Zheng, B.-Q. Xiong, Z. Wang, Y. Shen and X. Ren, *Journal of Materials Chemistry A* (2021).
- 52. X. Wu, J. J. Hong, W. Shin, L. Ma, T. Liu, X. Bi, Y. Yuan, Y. Qi, T. W. Surta, W. Huang, J. Neuefeind, T. Wu, P. A. Greaney, J. Lu and X. Ji, *Nature Energy*, **4**, 123 (2019).
- 53. H. Jiang, W. Shin, L. Ma, J. J. Hong, Z. Wei, Y. Liu, S. Zhang, X. Wu, Y. Xu, Q. Guo, M. A. Subramanian, W. F. Stickle, T. Wu, J. Lu and X. Ji, *Advanced Energy Materials*, **10**, 2000968 (2020).
- 54. T. Verhagen, J. Klimes, B. Pacakova, M. Kalbac and J. Vejpravova, ACS nano, 14, 15587 (2020).
- 55. A. Hakimian, M. Mohebinia, M. Nazari, A. Davoodabadi, S. Nazifi, Z. Huang, J. Bao and H. Ghasemi, *Nature communications*, **12**, 1 (2021).
- 56. X. Zhu, K. Wang, Y. Xu, G. Zhang, S. Li, C. Li, X. Zhang, X. Sun, X. Ge and Y. Ma, *Energy Storage Materials* (2021).
- 57. J. H. Park and N. Aluru, *Molecular Simulation*, **35**, 31 (2009).
- 58. J. Hao, J. Long, B. Li, X. Li, S. Zhang, F. Yang, X. Zeng, Z. Yang, W. K. Pang and Z. Guo, *Advanced Functional Materials*, **29**, 1903605 (2019).
- 59. J. Huang, X. Chi, Q. Han, Y. Liu, Y. Du, J. Yang and Y. Liu, *Journal of The Electrochemical Society*, **166**, A1211 (2019).
- 60. X. Zhang, J. Li, H. Ao, D. Liu, L. Shi, C. Wang, Y. Zhu and Y. Qian, *Energy Storage Materials*, **30**, 337 (2020).
- 61. Y. Gao, T. Rojas, K. Wang, S. Liu, D. Wang, T. Chen, H. Wang, A. T. Ngo and D. Wang, *Nature Energy*, **5**, 534 (2020).



Figure 1. Schematic illustration of key obstacles and strategies for low-temperature aqueous batteries.

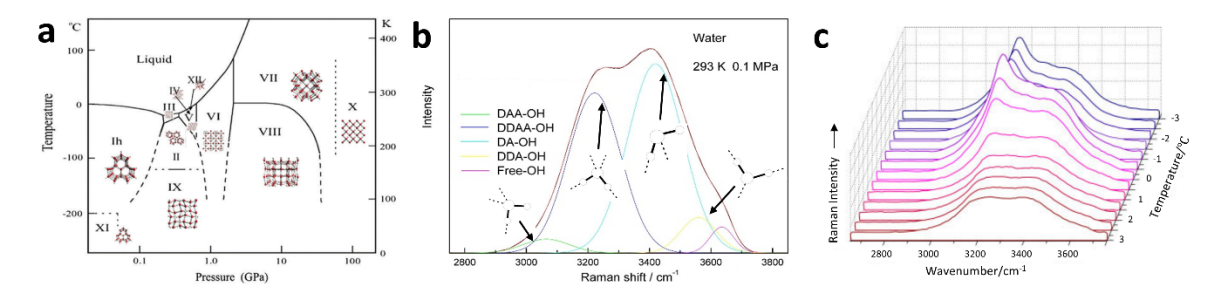


Figure 2. a) P-T phase diagram of pure water. Reproduced with permission from ref ¹⁴. Copyright 2018 Royal Society of Chemistry. b) Deconvoluted Raman O-H vibration peaks for different H-bonding configurations in pure water under ambient conditions, including DAA, DDAA, DA, DDA, and free water molecules, and their corresponding schematic structures. The thick lines represent the covalent bonds and the dashed lines represent the H-bonds. Reproduced with permission from ref ¹⁶. Copyright 2013 Elsevier. c) Raman spectra for water phase transformation from liquid to solid states. Reproduced with permission from ref ¹⁷. Copyright 2011 Wiley.

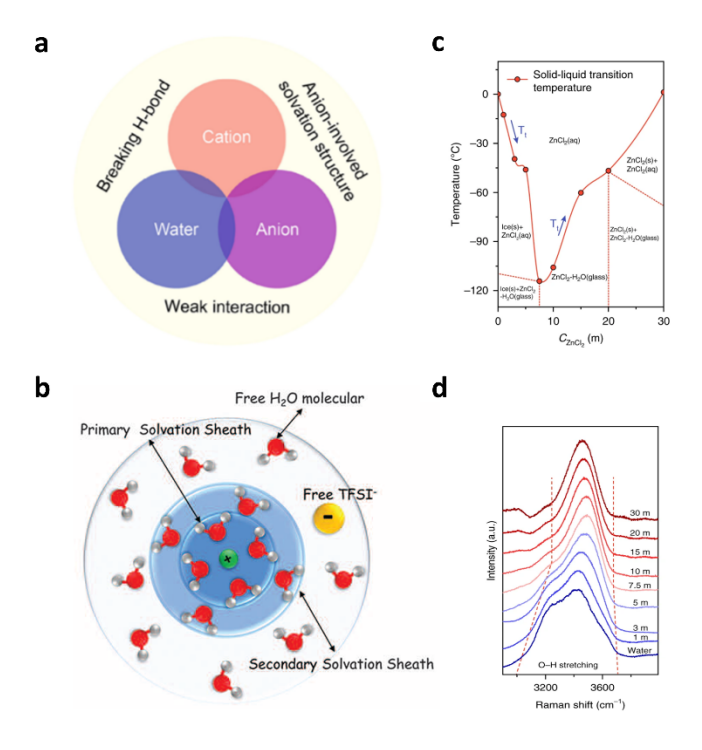


Figure 3. a) Schematic illustration of mutual interactions between cations, anions, and water solvents. Reproduced with permission from ref 39 . Copyright 2021 American Chemical Society. b) Schematic illustration of the cation solvation structure. Reproduced with permission from ref 29 . Copyright 2015 AAAS. c) Fitted temperature-composition phase diagram for $ZnCl_2$ aqueous electrolyte based on the data points shown in the Figure. Reproduced with permission from ref 32 . Copyright 2020 Springer Nature. d) Raman spectra showing the O-H stretching mode of $ZnCl_2$ aqueous electrolytes with the concentration ranging from 0 m to 30 m. Reproduced with permission from ref 32 . Copyright 2020 Springer Nature.

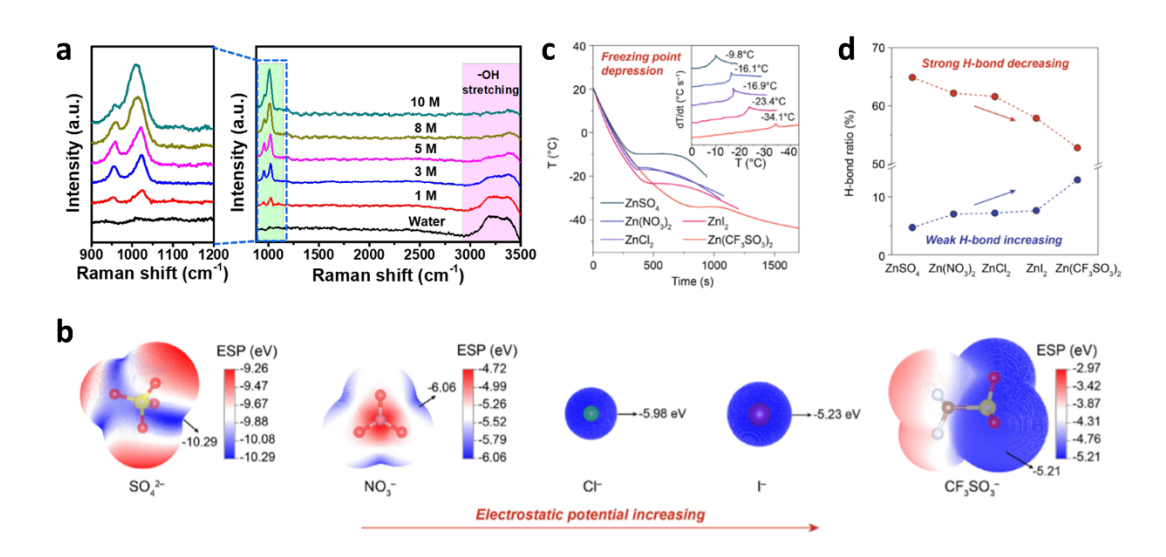


Figure 4. a) Raman spectra of H_2SO_4 aqueous electrolytes with the concentration ranging from 0 M to 10 M. Reproduced with permission from ref 31 . Copyright 2021 Wiley-VCH. b) DFT calculated ESP distribution in different anions. Reproduced with permission from ref 39 . Copyright 2014 American Chemical Society. c) Cooling curves for different electrolytes (inset shows their derived freezing points). Reproduced with permission from ref 39 . Copyright 2014 American Chemical Society. d) Statistical results of the strong and weak H-bonding ratios in different electrolytes. Reproduced with permission from ref 39 . Copyright 2014 American Chemical Society.

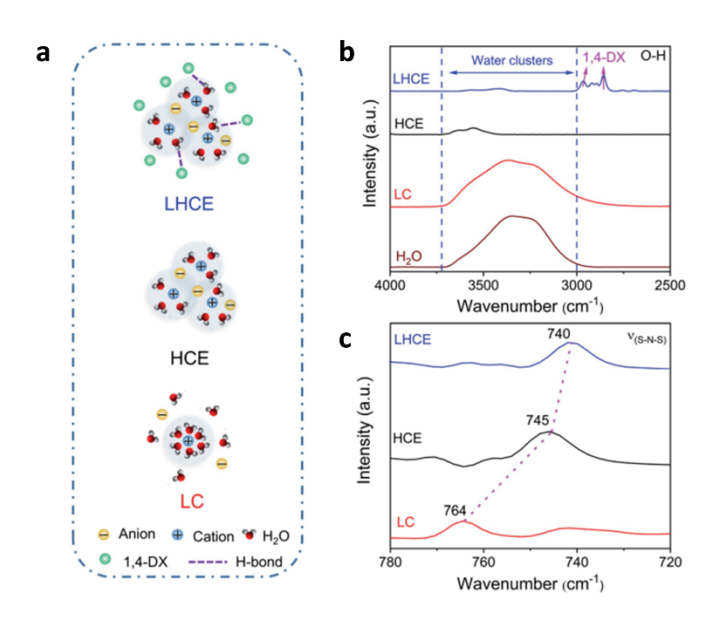


Figure 5. a) Schematic illustration for solvation structure in localized high-concentration electrolytes (LHCE), high-concentration electrolytes, and low concentration FTIR spectra for b) O-H, and c) S-N-S vibrations in different electrolytes. c)Reproduced with permission from ref ⁵¹. Copyright 2021 Royal Society of Chemistry.

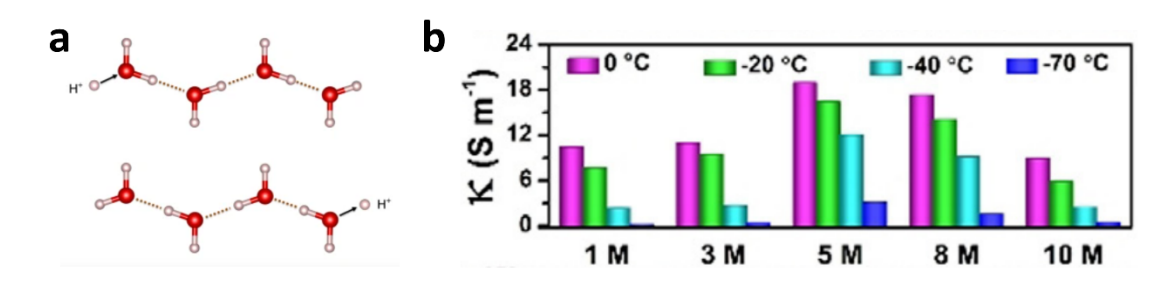


Figure 6. a) Schematic illustration of the Grotthuss mechanism for proton diffusion in aqueous electrolytes. Reproduced with permission from ref 52 . Copyright 2019 Springer Nature. b) Electrical conductivity of H_2SO_4 aqueous electrolytes of different concentrations and at different temperatures. Reproduced with permission from ref 31 . Copyright 2021 Wiley.

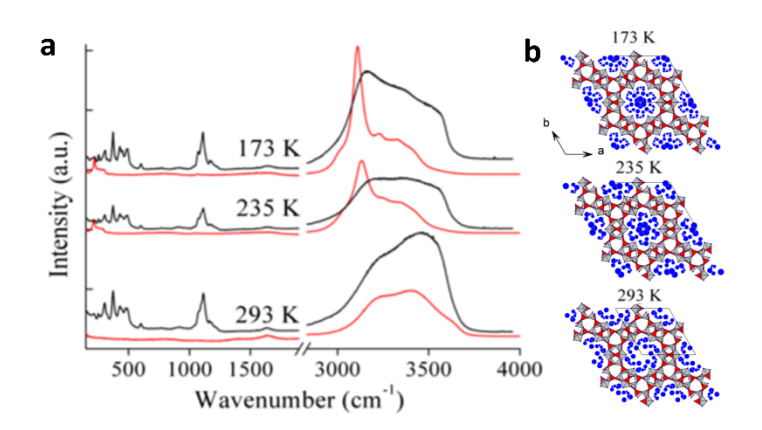


Figure 7. a) Raman spectra for space-confined water (black line) and bulk water (red line) O-H stretching band at different temperatures. b) Schematic structure transformation process of space-confined water from 293 K to 235 K, and to 173 K. Reproduced with permission from ref ²⁴. Copyright 2012 American Physical Society.